

**Unidirectional flow of solitons with nonlinearity management**M. O. D. Alotaibi <sup>1</sup>, S. M. Al-Marzoug,<sup>2</sup> H. Bahlouli,<sup>2</sup> and U. Al Khawaja <sup>3,\*</sup><sup>1</sup>*Department of Physics, Kuwait University, P.O. Box 5969 Safat, 13060 Kuwait*<sup>2</sup>*Department of Physics, King Fahd University of Petroleum and Minerals, Dhahran 31261, Saudi Arabia*<sup>3</sup>*Department of Physics, United Arab Emirates University, P.O. Box 15551, Al-Ain, United Arab Emirates* (Received 20 June 2019; revised manuscript received 12 September 2019; published 18 October 2019)

Unidirectional flow of solitons is obtained with a localized modulation of the nonlinearity strength. The modulation takes the shape of an asymmetric double well with a slight difference between the potential depths. The results were established using numerical computations and then verified qualitatively using a variational approach. Our results suggest that the most important physics at the origin of the unidirectional flow is the excitation of the breathing modes in the scattering region. Simplified variational equations of motion suggested that the phenomenon can be observed if the soliton is scattered by a generic asymmetric effective double potential well.

DOI: [10.1103/PhysRevE.100.042213](https://doi.org/10.1103/PhysRevE.100.042213)**I. INTRODUCTION**

The fascinating particlelike behavior of solitons stimulated interest at both the fundamental and technological levels. For instance, the interaction between solitons and their scattering centers was a prominent subject in soliton theory for the past few decades. Another example is the appealing features that solitons provide for optical data transfer and processing [1].

Unidirectional flow has been sought in many fields of applied physics including thermal, electromagnetic, acoustic waves [2–10], systems with  $PT$ -symmetric potentials [11–14], and metamaterials [15,16]. Using solitons in the all-optical data processing suggests that unidirectional flow of solitons is an essential element that needs to be established. Different schemes have been proposed for the discrete nonlinear Schrödinger equation (NLSE) with asymmetric nonlinearity [17] in waveguide arrays, double potential well for spatial solitons in the continuum [18], dispersion-managed waveguide arrays [19], and waveguide arrays with  $PT$ -symmetric potentials [14].

High efficiency performance was obtained in Ref. [18] with a double potential well with slightly different depths. It was pointed out in this reference that unidirectional flow of solitons occurs as a result of the combined effects of quantum reflection and exchange of energy between the center-of-mass and internal breathing modes. At the scattering point the breathing mode is excited with energy extracted from the center-of-mass kinetic energy. This reduces the group velocity slightly shifting it below the critical velocity for quantum reflection and hence the soliton reflects rather than transmits. Due to the asymmetry of the two potential wells, the soliton incoming from the other direction will not experience the same amount of group velocity reduction and thus will transmit. In this manner, only one direction of flow will be allowed for such a setup. In Ref. [19], a different scheme was followed

where the dispersion strength was modulated in the form of a double well function. Similar behavior was obtained as in the case of a double potential well. In the present paper, we address the third possibility, that is to modulate the strength of the nonlinearity.

It was established that the fundamental NLSE is integrable. Using a similarity transformation, or equivalently other methods, such as the existence of Lax Pair or Painlevé methods, the NLSE with varying coefficients was proven to be integrable only under certain integrability conditions that relate the different coefficients of the partial differential equation (PDE) to each other [20]. Hence, the strengths of the nonlinearity, dispersion, and potential terms in the NLSE were related to each other. The Riccati equation is an example of such a restriction [21]. Since unidirectional flow has been proven to occur with an asymmetric double well potential or a modulated dispersion, it would be natural to consider the third possibility of the integrability condition, namely the strength of the nonlinearity. In Ref. [17], this has been considered for a discrete system with two waveguides having different values. Here, we consider this problem for the continuum and show that indeed a highly efficient unidirectional flow can be obtained with nonlinearity modulation. From an application point of view, this scheme should be the most feasible as compared to the previous two since the nonlinearity of the medium can be modulated in an easier manner than for instance introducing a double potential well.

The model used here is the NLSE with position-dependent strength of the nonlinearity. The equation will be first solved numerically to show that asymmetric flow indeed exists. Then we develop a simplified variational approach that generates the effective equations of motion for the center-of-mass and breathing modes. The physics of the unidirectional flow will be exposed most clearly by considering the time dependence of the width of the soliton and its effect on the outcome of the scattering. Further insight will be attained by deriving an equation of motion for the center-of-mass motion which leads to the effective potential experienced by the soliton. It will

\*u.alkhawaja@uaeu.ac.ae

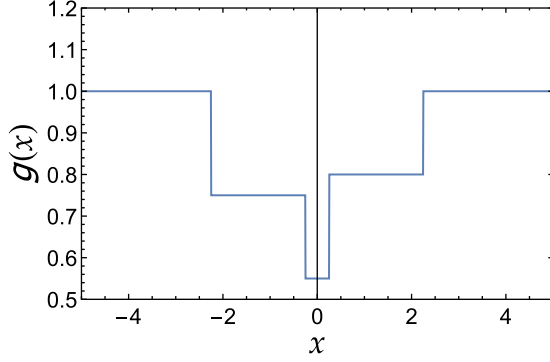


FIG. 1. Nonlinear coefficient as given by Eq. (2). Switching  $\delta$  from 1 to  $-1$  rotates the potential around the  $y$  axis. Here the parameters are  $g_0 = 1$ ,  $a_1 = 0.2$ ,  $a_2 = 0.25$ ,  $\alpha = 1.25$ , and  $\delta = 1$ .

be shown that the profile of this effective potential indeed changes depending on the direction from which the soliton approaches the potential.

In the next section, we present the theoretical model. Numerical results are presented in Sec. III. The variational calculation and its results are presented in Sec. IV. In Sec. V we discuss our results and conclude.

## II. THEORETICAL MODEL

In the absence of an external potential, the dynamics of a bright soliton is described by the following dimensionless nonlinear Schrödinger equation:

$$i \frac{\partial}{\partial t} \psi = -\frac{1}{2} \frac{\partial^2}{\partial x^2} \psi + g(x) |\psi|^2 \psi. \quad (1)$$

Here,  $\psi \equiv \psi(x, t)$  is the wave function and  $g(x)$  is the asymmetric potential-like nonlinear coefficient defined by

$$g(x) = g_0 - a_1 \Theta(\alpha - |x - \delta|) - a_2 \Theta(\alpha - |x + \delta|), \quad (2)$$

where  $\Theta(x)$  is the Heaviside function and the positive numbers  $a_{1,2}$ ,  $\delta$ ,  $\alpha$  define the depth, position, and width of the multiwell potential, depending on the choice of parameters. We have also considered other types of potential profiles such as the reflectionless sech-type asymmetric double well potential

$$g(x) = g_0 - a_1 \operatorname{sech}^2\left(\frac{x}{\alpha}\right) - a_2 \operatorname{sech}^2\left(\frac{x}{\alpha}\right). \quad (3)$$

While Eq. (2) will be used for the variational calculation and numerical simulations throughout this paper, Eq. (3) is used in the numerical solution to verify the existence of the unidirectional flow for different shapes of potential. The main advantage of the above engineered square well potential stems from its ease in handling the necessary space integrations required to obtain the effective Lagrangian. In Fig. 1, we plot  $g(x)$  for  $a_1 = 0.2$ ,  $a_2 = 0.25$ ,  $\alpha = 1.25$ ,  $g_0 = 1$ , and  $\delta = 1$ . Note that when we change  $\delta$  from 1 to  $-1$  we rotate the potential around  $x = 0$ . Therefore, an equivalent procedure to change the launching direction of soliton from right to left of the potential is to fix the launching point on one side of the potential and study the scattering by changing the sign of  $\delta$  from  $\delta = 1$  to  $-1$ .

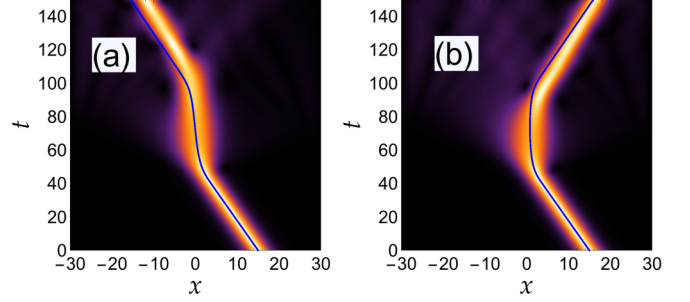


FIG. 2. Spatiotemporal plot for a soliton scattered by the region of modulated nonlinearity strength. (a)  $\delta = 1$  corresponding to a soliton incident from the right. (b)  $\delta = -1$  equivalent to a soliton incident from the left. Solid blue line is the trajectory obtained using the variational calculation. Parameters are  $x_0(0) = 15$  and  $v = -0.25$ .

As an initial soliton profile, we use the exact bright soliton solution of Eq. (1) with constant nonlinearity  $g(x) = g_0$ ,

$$\psi(x, t) = \frac{n \sqrt{g_0}}{2} \operatorname{sech}\left(\frac{1}{2} n g_0 (x - x_0 - v_0 t)\right) \times e^{i[v(x-x_0) + (n^2 g_0^2 - 4v_0^2)t/8]}, \quad (4)$$

with  $x_0$ ,  $v_0$ , and  $n$ , being the initial position, group velocity, and norm, respectively. Transport coefficients are calculated using the following formulas:

$$R = \frac{1}{n} \int_{\delta+\alpha}^{\infty} |\psi(x, t_f)|^2 dx, \quad (5)$$

for the reflectance, where  $t_f$  is a time scale long after the scattering such that the soliton restores its state of uniform steady flow far away from the scattering potential. For the transmittance we have

$$T = \frac{1}{n} \int_{-\infty}^{-\delta-\alpha} |\psi(x, t_f)|^2 dx, \quad (6)$$

and finally for the trapping

$$L = \frac{1}{n} \int_{-\delta-\alpha}^{\delta+\alpha} |\psi(x, t_f)|^2 dx. \quad (7)$$

Probability conservation law requires that  $R + T + L = 1$ .

## III. NUMERICAL RESULTS

Normally, the unidirectional flow is investigated by launching a soliton towards the region of modulated nonlinearity strength from both sides and observe the scattered soliton in each case. Equivalently, we may keep fixed the launching point, say on the right hand side, and then reflect the modulation function with respect to the vertical axis in Fig. 1 by switching  $\delta$  from positive to negative value. This will reproduce the potential shown in Fig. 1 but reflected with respect to the  $x = 0$  vertical axis.

Our first result in Fig. 2 shows clearly that indeed a unidirectional flow is obtained by switching the sign of  $\delta$  from 1 to  $-1$ . It is noticed that in both cases the soliton preserves its integrity after scattering. The corresponding transport coefficients are shown in Figs. 3 and 4. In Fig. 3, we used the

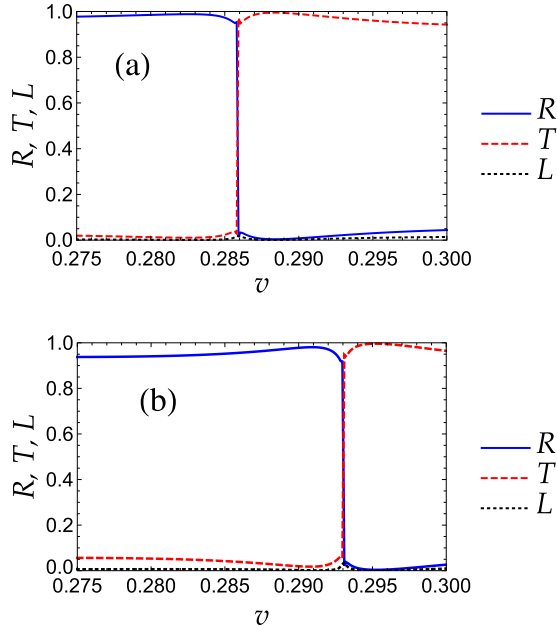


FIG. 3. Transport coefficients obtained from the numerical solution of the NLSE, Eq. (1), for  $\delta = -1$  (a) and  $\delta = 1$  (b) with the reflectionless potential well, Eq. (3).

reflectionless double well potential, Eq. (3), and in Fig. 4 we used the square potential well, Eq. (2). It is clear from Fig. 3 that a sharp transition from almost full reflectance to full transmittance takes place at the critical group velocity of  $v \approx 0.285$ . The transition in Fig. 4 is not as sharp as in Fig. 3 due to the nonreflectionless nature of the square potential well which causes some radiation upon scattering. Furthermore, trapping is absent from the reflectionless case while it occurs for the square potential well around the transition region. While in general there is full trapping near the transitions, there is still a window in the soliton speed where trapping is very small and unidirectional flow takes place. Comparing

the reflectance in both cases of positive and negative  $\delta$ , we find in Figs. 3 and 4 a velocity window  $[0.286, 0.293]$  and  $[0.282, 0.287]$ , respectively, within which the unidirectional flow takes place.

To understand qualitatively the physics of the unidirectional flow, we develop in the next section a variational approach. This will enable us to verify that the excitation of the internal modes is the essential mechanism that ensures the unidirectional flow.

#### IV. VARIATIONAL CALCULATIONS

In this section, we study the interaction between the bright soliton with the asymmetric double well nonlinearity coefficient using the variational method. The Lagrangian density associated with Eq. (1) is

$$\mathcal{L} = \frac{i}{2} \left[ \psi^* \frac{\partial \psi}{\partial t} - \psi \frac{\partial \psi^*}{\partial t} \right] - \frac{1}{2} \left| \frac{\partial \psi}{\partial x} \right|^2 - \frac{1}{2} g(x) |\psi|^4, \quad (8)$$

where we can use the Euler-Lagrange equation of motion to obtain Eq. (1).

We adopt the following trial function as the variational bright soliton solution to Eq. (1),

$$\psi(x, t) = A \operatorname{sech} \left[ \frac{(x - x_0)}{w} \right] \times \exp \{ i [\phi_0 + (x - x_0)\phi_1 + (x - x_0)^2\phi_2] \}. \quad (9)$$

The variational parameters  $A(t)$ ,  $x_0(t)$ ,  $w(t)$ ,  $\phi_0(t)$ ,  $\phi_1(t)$ , and  $\phi_2(t)$  represent the amplitude, center-of-mass position, width, phase, velocity, and the chirp of the soliton, respectively. We may reduce the number of variational parameters by 1 when we use the normalization condition,

$$\int_{-\infty}^{\infty} dx |\psi|^2 = 2A^2w = n. \quad (10)$$

Substituting the trial function, Eq. (9), into the Lagrangian density, Eq. (8), using Eq. (2) for the nonlinearity profile, and then integrating over space from  $-\infty$  to  $\infty$  results in the effective Lagrangian as a function of the variational parameters,

$$\begin{aligned} L = & -\frac{n^2 a_2}{24w} \left\{ \left[ 2 + \operatorname{sech}^2 \left( \frac{-\alpha + \delta + x_0}{w} \right) \right] \tanh \left( \frac{-\alpha + \delta + x_0}{w} \right) - \left[ 2 + \operatorname{sech}^2 \left( \frac{\alpha + \delta + x_0}{w} \right) \right] \tanh \left( \frac{\alpha + \delta + x_0}{w} \right) \right\} \\ & + \frac{n^2 a_1}{24w} \left\{ \left[ 2 + \operatorname{sech}^2 \left( \frac{\alpha + \delta - x_0}{w} \right) \right] \tanh \left( \frac{\alpha + \delta - x_0}{w} \right) + \left[ 2 + \operatorname{sech}^2 \left( \frac{\alpha - \delta + x_0}{w} \right) \right] \tanh \left( \frac{\alpha - \delta + x_0}{w} \right) \right\} \\ & - \frac{n}{6w^2} - \frac{g_0 n^2}{6w} - \frac{1}{2} n \phi_1^2 - \frac{1}{6} n \pi^2 w^2 \phi_2^2 + n \phi_1 dx_0/dt - n d\phi_0/dt - \frac{1}{12} n \pi^2 w^2 d\phi_2/dt. \end{aligned} \quad (11)$$

Applying the Euler-Lagrange equations for each of the variational parameters yields a system of ordinary differential equations that describes their time evolution. Most of these equations are lengthy and hence we relegate the writing of the explicit system of equations of motion to the Appendix.

In Fig. 2, we plot the trajectory of the soliton calculated from the variational approach (solid blue line) showing a very good agreement with the numerical calculations. Transport coefficients are shown in Figs. 3 and 4. Very sharp transitions

occur at the critical velocity and a unidirectional window indeed exists.

The transport coefficients, given by Eqs. (5)–(7), can be calculated, from the variational calculation, as follows:

$$\begin{aligned} R = & \frac{1}{2n} \lim_{D \rightarrow \infty} \left[ \tanh \left( \frac{D - x_0(t_f)}{w(t_f)} \right) \right. \\ & \left. - \tanh \left( \frac{\alpha + \delta - x_0(t_f)}{w(t_f)} \right) \right], \end{aligned} \quad (12)$$

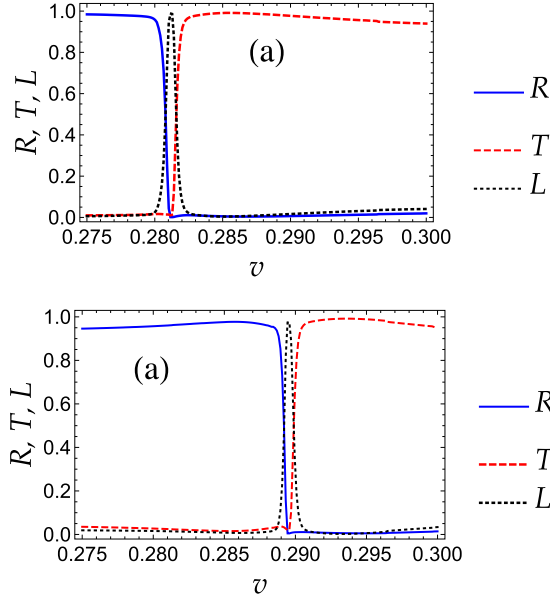


FIG. 4. Transport coefficients obtained from the numerical solution of the NLSE, Eq. (1), for  $\delta = -1$  (a) and  $\delta = 1$  (b) with the double square potential well, Eq. (2).

$$T = \frac{1}{2n} \lim_{D \rightarrow \infty} \left[ \tanh \left( \frac{D + x_0(t_f)}{w(t_f)} \right) - \tanh \left( \frac{\alpha + \delta + x_0(t_f)}{w(t_f)} \right) \right], \quad (13)$$

$$L = \frac{1}{2n} \lim_{D \rightarrow \infty} \left[ \tanh \left( \frac{\alpha + \delta - x_0(t_f)}{w(t_f)} \right) + \tanh \left( \frac{\alpha + \delta + x_0(t_f)}{w(t_f)} \right) \right]. \quad (14)$$

At large time,  $t = t_f$ , the soliton is far from the scattering region,

$$x_0(t_f) \rightarrow \begin{cases} D, & \delta = -1 \\ -D, & \delta = 1 \end{cases}, \quad (15)$$

where  $D$  is large compared to the scattering region  $\alpha$  and soliton width  $\alpha w(t)$ . This is verified in Fig. 5, where we plot

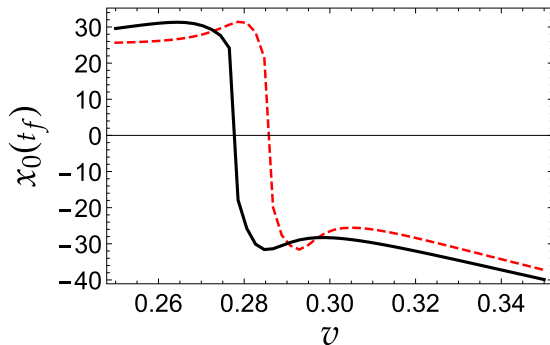


FIG. 5. Soliton position long after scattering ( $t_f = 200$ ) vs initial group velocity. Solid curve corresponds to  $\delta = -1$  and dashed curve corresponds to  $\delta = 1$ .

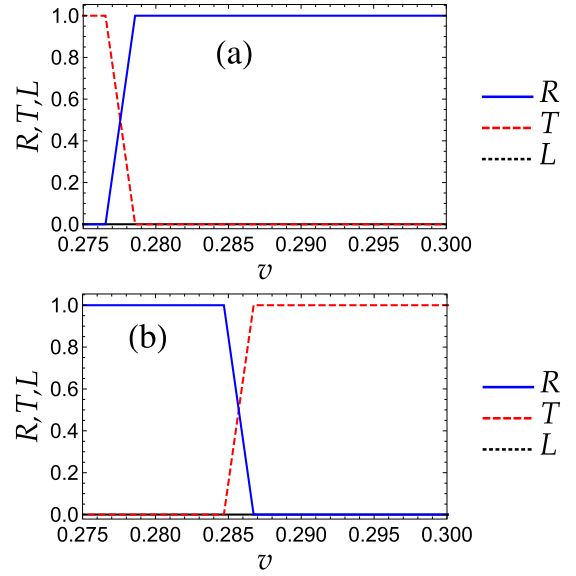


FIG. 6. Transport coefficients obtained from the variational calculation for  $\delta = -1$  (a) and  $\delta = 1$  (b).

$x_0(t_f)$  versus the velocity of incidence  $v$ . Here again, unidirectional flow is evident within a velocity window near the critical speed. Using the asymptotic forms of  $\lim_{x \rightarrow \pm\infty} \tanh(x) = \pm 1$ , the reflection transport coefficient within the unidirectional flow window takes the form

$$R = \begin{cases} 1, & \delta = -1 \\ 0, & \delta = 1 \end{cases}, \quad (16)$$

which is the ideal mathematical form of unidirectional flow. In Fig. 6, we plot the transport coefficients using the variational calculation. The sharpness in the transitions at the critical speed is indicated by the sharp transition in  $x_0(t_f)$  as explained above and shown in Figs. 3 and 4.

In conclusion, the variational calculation describes accurately the dynamics of the scattered soliton and accounts for the unidirectional flow. A necessary condition for the variational calculation to account for the unidirectional flow is to allow the width to change with time. Setting the width as constant leads to the disappearance of unidirectional flow. With a time-dependent width and its conjugate variable, the chirp, the equations of motion become complicated as shown in the Appendix. In order to give more insight into the dynamics, we simplify the equations of motion in the next section to reduce the problem to a soliton scattered by an effective asymmetric potential.

### Simplified dynamics and effective potential

The main aim of the variational calculation is to capture the physics of unidirectional flow. To that end, we simplify the rather lengthy and complicated variational equations of motion. The simplification is performed by first noting that away from the scattering region, the soliton is not anymore affected by the nonlinearity modulation and hence will be moving with a uniform speed. Then, we expand the equations in the small quantity  $w(t)/x_0(t)$ . This will give accurate behavior at the asymptotes—long before and long after the scattering—

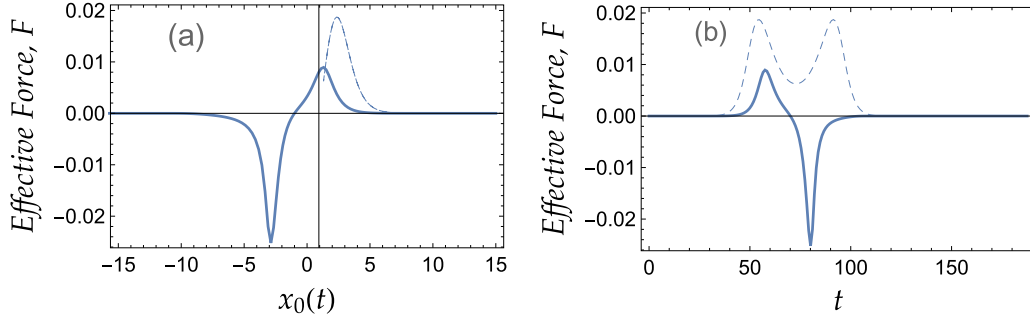


FIG. 7. Effective force, given by Eq. (22). Dashed curve corresponds to  $\delta = -1$  and solid curve corresponds to  $\delta = 1$ .

but a less accurate account near the scattering region since  $w(t)/x_0(t)$  is not small there. However, by comparing the results of the simplified equations of motion to those of the exact ones, it turned out that this is an acceptable approximation. Most importantly, it captures the main features of the unidirectional flow and furthermore provides a description of the dynamics in terms of soliton scattered by an effective potential that changes its profile depending on the direction from which the soliton is incident on the potential. Based on the above approximation, the simplified equations of motion take the following form:

$$x'_0(t) - \phi_1(t) = 0, \quad (17)$$

$$w'(t) - 2w(t)\phi_2(t) = 0, \quad (18)$$

$$\frac{a_2 n \left[ \operatorname{sech}^2\left(\frac{\alpha + \delta - x_0(t)}{w(t)}\right) - \operatorname{sech}^2\left(\frac{-\alpha + \delta - x_0(t)}{w(t)}\right) \right]}{12w(t)^2} - \phi'_1(t) = 0, \quad (19)$$

$$\frac{a_1 n x_0(t) \operatorname{sech}^2\left(\frac{2[\delta + x_0(t)]}{w(t)}\right)}{2w(t)^3} + \frac{g_0 n}{6w(t)^2} - \frac{1}{6}\pi^2 w(t)\phi'_2(t) - \frac{1}{3}\pi^2 w(t)\phi_2(t)^2 + \frac{1}{3w(t)^3} = 0. \quad (20)$$

Equations (17) and (19) show that the trajectory of the soliton satisfies the effective Newton's equation

$$\ddot{x}_0 = F[x_0], \quad (21)$$

where

$$F[x_0] = \frac{a_2 n \left[ \operatorname{sech}^2\left(\frac{\alpha + \delta - x_0}{w}\right) - \operatorname{sech}^2\left(\frac{-\alpha + \delta - x_0}{w}\right) \right]}{12w^2} \quad (22)$$

is an effective *force* experienced by the soliton. The associated effective potential can be calculated using

$$V[x_0] = - \int F[x_0] dx_0. \quad (23)$$

In performing this integration, it should be noted that  $w(t)$  depends also on  $x_0$ . Equations (18) and (20) can be used to eliminate  $\phi_2$  and then solve for  $w(t)$  in terms of  $x_0(t)$ . As this will produce a complicated expression for the resulting potential, we would rather calculate the effective potential numerically, as detailed below. Nonetheless, further insight about the physics behind the unidirectional flow mechanism can be obtained by additional simplifications of the equations of motion in the regions away from the scattering point. For  $x_0$  much larger than  $\alpha$  and  $w$ , the right hand side of Eq. (22) is approximated by

$$F[x_0] = 2\alpha \operatorname{sech}^4(x_0) \{2\delta [\cosh(2x_0) - 2] + \sinh(2x_0)\}, \quad (24)$$

which upon integrating with respect to  $x_0$  gives the potential

$$V[x_0] = 2\alpha \operatorname{sech}^2(x_0) [1 + 2\delta \tanh(x_0)]. \quad (25)$$

This is the asymptotic potential at large  $x_0$  experienced by the scattered soliton. For a soliton incident from the right with  $\delta = 1$ , it will experience a potential  $\propto \tanh[x_0(t)]$ , which is a step potential with value before the scattering higher than after the scattering and thus the soliton will cross the origin and transmit, as found in the full numerical solution. For a soliton incident again from the right but with  $\delta = -1$ , the soliton will experience a potential  $\propto -\tanh[x_0(t)]$ , which is again a step function but with value before scattering lower than after scattering explaining the soliton reflection in this case. In conclusion, it is the asymmetry introduced by the potential that leads to the difference in the scattering outcome.

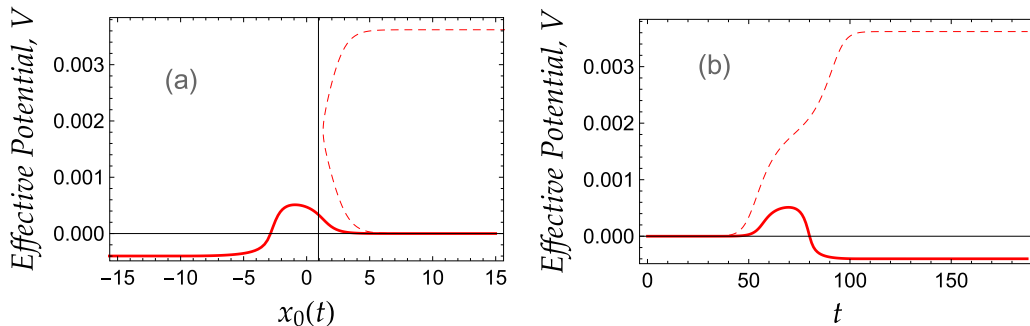


FIG. 8. Effective potential. Dashed curve corresponds to  $\delta = -1$  and solid curve corresponds to  $\delta = 1$ .

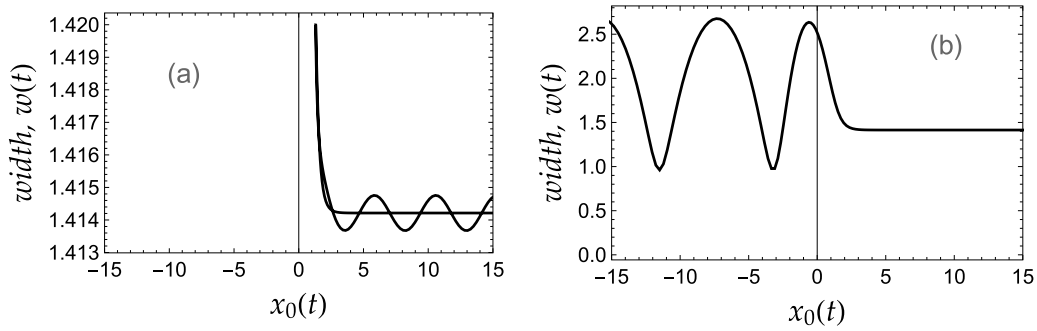


FIG. 9. Soliton width. Left panel corresponds to  $\delta = -1$  and right panel corresponds to  $\delta = 1$ .

In Fig. 7, we plot the effective force, given by Eq. (22), versus the soliton position  $x_0(t)$ . Both cases where the soliton is incident from the right and from the left are considered. For a soliton incident from the right which amounts to  $\delta < 0$ , the dashed curve in Fig. 7 shows that the soliton encounters a repulsive force that forces it to reflect. The solid curve shows that when the soliton is incident from the left it encounters a considerably less repulsive force followed by a larger attractive force and thus transmits with an increase in its speed.

In Fig. 8, we plot the effective potential for both positive and negative values of  $\delta$ . For  $\delta < 0$ , which amounts to a soliton incident from the right, the soliton will experience a high effective potential barrier that forces it to reflect. On the other hand, for  $\delta > 0$ , which corresponds to a soliton incident from the left, the soliton will encounter a smaller potential barrier through which it transmits. Plotting in this figure the potential versus time shows that the soliton experiences a potential step for a soliton incident from the right and a considerably smaller potential barrier for a soliton incident from the left. The width of the soliton is plotted in Fig. 9. It shows that in both cases of reflectance and transmittance, the soliton acquires oscillations in its width. However, the amplitude of width oscillation is much larger for the transmission case. The speed of the soliton is plotted in Fig. 10 showing that there is an increase in the speed in the case of transmission. The increase in speed shifts the speed of the soliton from below the critical to above the critical speed for transmission.

**V. CONCLUSIONS**

We have considered the scattering of a bright soliton off a region of modulated nonlinearity strength. The modulation

takes the form of an asymmetric double well potential, the two wells have the same width but slightly different depths. The numerical solution shows that this setup indeed leads to a unidirectional flow within a window of soliton speed. To understand the mechanism of this behavior, we derived through a variational calculation the effective equations of motion for the soliton’s peak position, speed, width, and chirp. It was shown that transmission takes place when the soliton undergoes considerable width oscillations as a result of its scattering. This is in contrast with the case of reflection where the width of the soliton remains constant. This leads to the fact that the excitation of the internal breathing mode is a crucial factor in the realization of the unidirectional flow. Furthermore, it was noticed that upon transmission the soliton emerges with an increase in the speed while upon reflection its speed is the same as before scattering. A simplified version of the equations of motion reveals that during transmission, the soliton experiences a net attractive force that gives rise to the speed increase. The reflected soliton does not experience such an attractive force and thus reflects with the speed of incidence. This mechanism is different from that in Ref. [18] where NLSE was considered with modulated dispersion. In that work, the speed of the soliton was reduced after transmittance. This difference in unidirectional flow mechanism can be understood by invoking the integrability condition of the NLSE with space variable coefficients, as derived by Ref. [20]. For a dispersion coefficient  $f(x, t)$  and nonlinearity coefficient  $g(x, t)$ , the integrability condition reads  $f(x, t) = c(t)/g(x, t)^2$ , where  $c(t)$  is an arbitrary real function. Thus, for integrability of the NLSE to be preserved, the modulation in dispersion should have the inverse effect of the modulation in nonlinearity.

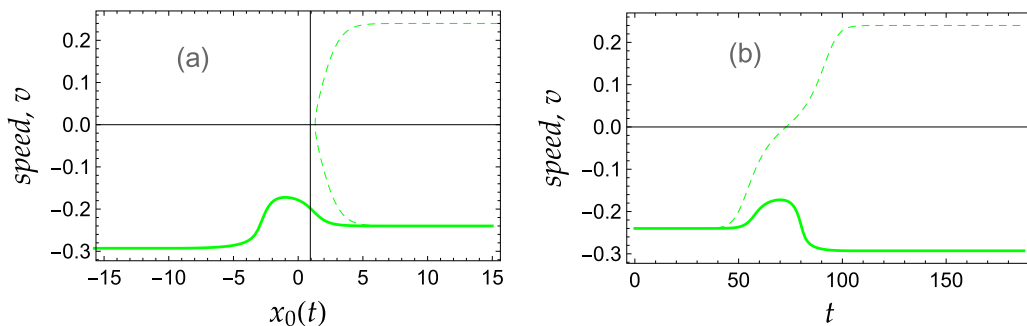


FIG. 10. Soliton speed. Dashed curve corresponds to  $\delta = -1$  and solid curve corresponds to  $\delta = 1$ .

We would like to stress that our results are in agreement with recent references [22–24] which studied the necessary conditions for nonreciprocal plane wave propagation in nonlinear media. These results remain valid for soliton propagation in modulated NLSE.

Our trial function (9) does not account for a trapped part. In Ref. [25], the authors used a variational calculation with a trial function that accounts for both the incident soliton and a trapped part. This allowed for the detailed study of resonant interaction between the incident soliton and the bound states of the potential well. While accounting for a trapped part would, in principle, enhance our calculations, it will not affect the regions away from the sharp transition in the transport coefficients. Since the unidirectional flow takes place for soliton speeds away from the critical values where the sharp transitions occur, we believe that adding a trapped part will not have significant effect on our results. However, this may be left for future investigation.

In the present work, we employed an asymmetric square double potential well. Ideally, one should use reflectionless

potentials to minimize radiative losses. Nonetheless, it turned out that even with the square double potential well used, the efficiency of the unidirectional flow obtained is still very high.

We believe that our findings will be of great interest and may have applications in optical data transmission in fibers or data processing in waveguide arrays.

### ACKNOWLEDGMENTS

U.A.K. and H.B. acknowledge the support of King Fahd University of Petroleum and Minerals. We also acknowledge the support of the Saudi Center for Theoretical Physics (SCTP). U.A.K. acknowledges the support of Grants No. UAEU-UPAR(4) 2016 and No. UAEU-UPAR(6) 2017.

### APPENDIX: VARIATIONAL EQUATIONS OF MOTION

Using the effective Lagrangian, Eq. (11), the Euler-Lagrange equations lead to the following variational equations of motion:

$$\begin{aligned}
 & -\frac{n^2 a_1}{24w^2} \left\{ \tanh\left(\frac{\alpha + \delta - x_0}{w}\right) \left[ 2 + \operatorname{sech}\left(\frac{\alpha + \delta - x_0}{w}\right)^2 \right] + \tanh\left(\frac{\alpha - \delta + x_0}{w}\right) \left[ 2 + \operatorname{sech}\left(\frac{\alpha - \delta + x_0}{w}\right)^2 \right] \right. \\
 & \left. + \frac{3}{w} \left[ \operatorname{sech}\left(\frac{\alpha + \delta - x_0}{w}\right)^4 (\alpha + \delta - x_0) + \operatorname{sech}\left(\frac{\alpha - \delta + x_0}{w}\right)^4 (\alpha - \delta + x_0) \right] \right\} \\
 & + \frac{n^2 a_2}{24w^2} \left\{ \tanh\left(\frac{-\alpha + \delta + x_0}{w}\right) \left[ 2 + \operatorname{sech}\left(\frac{-\alpha + \delta + x_0}{w}\right)^2 \right] - \tanh\left(\frac{\alpha + \delta + x_0}{w}\right) \left[ 2 + \operatorname{sech}\left(\frac{\alpha + \delta + x_0}{w}\right)^2 \right] \right. \\
 & \left. + \frac{3}{w} \left[ \operatorname{sech}\left(\frac{-\alpha + \delta + x_0}{w}\right)^4 (-\alpha + \delta + x_0) - \operatorname{sech}\left(\frac{\alpha + \delta + x_0}{w}\right)^4 (\alpha + \delta + x_0) \right] \right\} + \frac{n^2 g_0}{6w^2} + \frac{n}{3w^3} - \frac{1}{3} n\pi^2 w \phi_2^2 \\
 & - \frac{1}{6} n\pi^2 w \frac{d}{dt} \phi_2 = 0,
 \end{aligned} \tag{A1}$$

$$\begin{aligned}
 & \frac{n^2 a_2}{8w^2} \left[ -\operatorname{sech}\left(\frac{-\alpha + \delta + x_0}{w}\right)^4 + \operatorname{sech}\left(\frac{\alpha + \delta + x_0}{w}\right)^4 \right] + \frac{n^2 a_1}{8w^2} \left[ -\operatorname{sech}\left(\frac{\alpha + \delta - x_0}{w}\right)^4 + \operatorname{sech}\left(\frac{\alpha - \delta + x_0}{w}\right)^4 \right] \\
 & - n \frac{d}{dt} \phi_1 = 0,
 \end{aligned} \tag{A2}$$

$$-\frac{1}{3} n\pi^2 w^2 \phi_2 + \frac{1}{6} n\pi^2 w \frac{d}{dt} w = 0, \tag{A3}$$

$$-n\phi_1 + n \frac{d}{dt} x_0 = 0. \tag{A4}$$

[1] A. Hasegawa and Y. Kodama, *Solitons in Optical Communications* (Oxford University Press, New York, 1995); L. F. Mollenauer and J. P. Gordon, *Solitons in Optical Fibers* (Academic, Boston, 2006); G. P. Agrawal, *Nonlinear Fiber Optics*, 3rd ed. (Academic, San Diego, 2001); N. N. Akhmediev and A. Ankiewicz, *Solitons: Nonlinear Pulses and Beams* (Chapman and Hall, London, 1997).

[2] M. Terraneo, M. Peyrard, and G. Casati, *Phys. Rev. Lett.* **88**, 094302 (2002).  
 [3] D. Segal and A. Nitzan, *Phys. Rev. Lett.* **94**, 034301 (2005).  
 [4] C. W. Chang, D. Okawa, A. Majumdar, and A. Zettl, *Science* **314**, 1121 (2006).  
 [5] W. Kobayashi, Y. Teraoka, and I. Terasaki, *Appl. Phys. Lett.* **95**, 171905 (2009).

- [6] M. Scalora, J. P. Dowling, C. M. Bowden, and M. J. Bloemer, *J. Appl. Phys.* **76**, 2023 (1994).
- [7] M. D. Tocci, M. J. Bloemer, M. Scalora, J. P. Dowling, and C. M. Bowden, *Appl. Phys. Lett.* **66**, 2324 (1995).
- [8] K. Gallo, G. Assanto, K. Parameswaran, and M. Fejer, *Appl. Phys. Lett.* **79**, 314 (2001).
- [9] V. F. Nesterenko, C. Daraio, E. B. Herbold, and S. Jin, *Phys. Rev. Lett.* **95**, 158702 (2005).
- [10] H.-X. Sun, S.-Y. Zhang, and X.-J. Shui, *Appl. Phys. Lett.* **100**, 103507 (2012).
- [11] Z. Lin, H. Ramezani, T. Eichelkraut, T. Kottos, H. Cao, and D. N. Christodoulides, *Phys. Rev. Lett.* **106**, 213901 (2011).
- [12] H. Ramezani, T. Kottos, R. El-Ganainy, and D. N. Christodoulides, *Phys. Rev. A* **82**, 043803 (2010).
- [13] N. Bender, S. Factor, J. D. Bodyfelt, H. Ramezani, D. N. Christodoulides, F. M. Ellis, and T. Kottos, *Phys. Rev. Lett.* **110**, 234101 (2013).
- [14] U. Al Khawaja, S. M. Al-Marzoug, H. Bahlouli, and Y. S. Kivshar, *Phys. Rev. A* **88**, 023830 (2013).
- [15] M. W. Feise, I. V. Shadrivov, and Y. S. Kivshar, *Phys. Rev. E* **71**, 037602 (2005).
- [16] L. Feng, Y.-L. Xu, W. S. Fegadolli, M.-H. Lu, J. E. B. Oliveira, V. R. Almeida, Y.-F. Chen, and A. Scherer, *Nat. Mater.* **12**, 108 (2012).
- [17] S. Lepri and G. Casati, *Phys. Rev. Lett.* **106**, 164101 (2011).
- [18] U. Al Khawaja and M. Asad-Uz-Zaman, *Europhys. Lett.* **101**, 50008 (2013).
- [19] U. Al Khawaja and A. A. Sukhorukov, *Opt. Lett.* **40**, 2719 (2015).
- [20] U. Al Khawaja, *J. Math. Phys.* **51**, 053506 (2010).
- [21] V. N. Serkin and A. Hasegawa, *IEEE J. Sel. Top. Quantum Electron.* **8**, 418 (2002).
- [22] G. Wu, Y. Long, and J. Ren, *Phys. Rev. B* **97**, 205423 (2018).
- [23] H. Yan, G. Wu, and J. Ren, *Phys. Rev. E* **100**, 012207 (2019).
- [24] N. Li and J. Ren, *Sci. Rep.* **4**, 6228 (2014).
- [25] T. Ernst and J. Brand, *Phys. Rev. A* **81**, 033614 (2010).